a good fit of the Table 7 data to the MGB TD for which t = 0 years. A linear scaling of the r/R_s values in Table 7 to larger "original" values, call them $(r/R_s)'$, that existed at t = 0 years is assumed:

$$(r/R_s)' = - a + (a + 1)(r/R_s), \tag{8}$$

where a is an adjustable constant. This form for the scaling equation ensures that orbital radii of satellites and rings that are close to Saturn's surface are not altered very much. (Note: When $(r/R_s) =1$ so does $(r/R_s)'$). Also the larger the orbital radius the larger the alteration. Subsequently the $(r/R_s)'$ values, not the r/R_s values, are used in the fitting process. Perhaps, if the MGB TD's in Fig. 15 were to be linearly compressed by reasonably altering parameters used to calculate these TD's, it would not be necessary to transform orbital radii by means of Eq. (8).

2.8.a. Fitting the MGB TD for which t = 0 years

The data from Table 7 is used to fit the MGB t = 0 year TD by adjusting the constant a in Eq. (8) along with C'_1 and C'_2. The best fit parameters are $a = 2.20$, $C_1' = 1.080$ K•cm and $C_2' = - 462$ cm^{-1}. The best fit to the t = 0 year TD is in Fig. 17.

Fig. 17. The best fit to any MGB TD is achieved by transforming satellite r/R_s values to $(r/R_s)'$ values. This MGB TD corresponds t = 0 years.

Figure 17

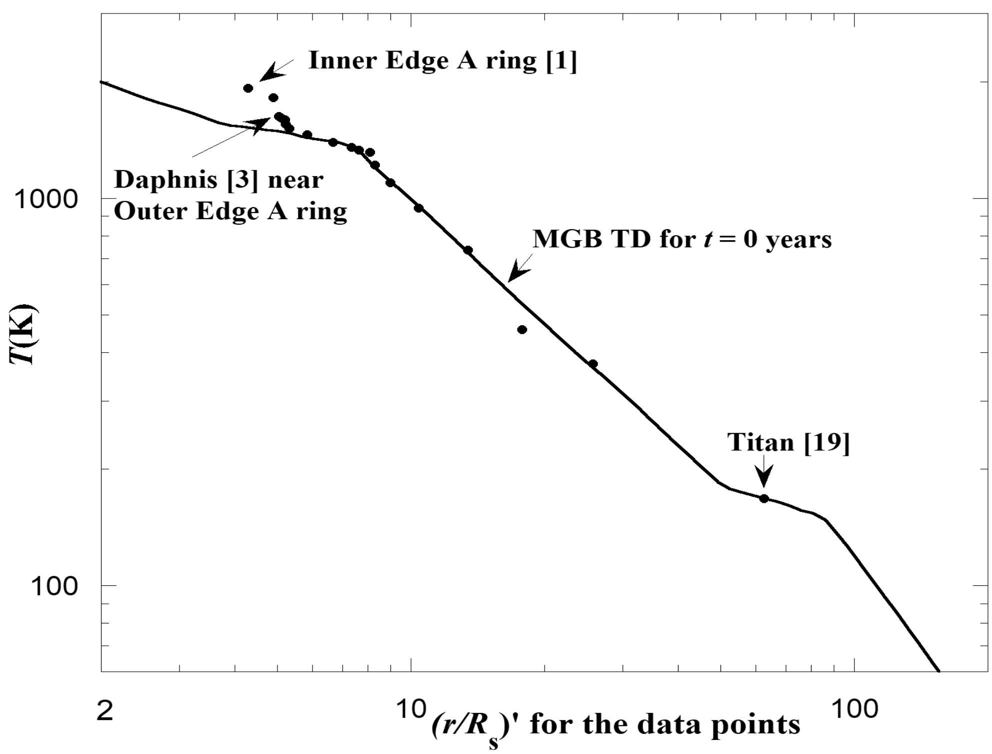

Eq. (7) and the best fit parameters are used with Table 9 to determine the complete Saturnian disk TD seen in Fig. 18. Also shown there is the MGB TD for which $t = 0$ years. The complete TD found in the present investigation has a peak just as in the Uranian disk TD. Note the present model TD diverges from the MGB TD in the region of Saturn's A ring which is positioned on the side of the peak. This divergence is similar to one in the Uranian and Neptunian disk TD's in Fig. 10. Additionally, just up from the points of divergence there is a small shoulder in the side of the TD's peak. This is reminiscent of the small shoulder in a similar spot in Fig. 10 the composite TD for the disks of Uranus Jupiter and Neptune.

Fig. 18. The overlap of the complete Saturnian TD from the present investigation with the MGB TD for which *t* = 0 years.

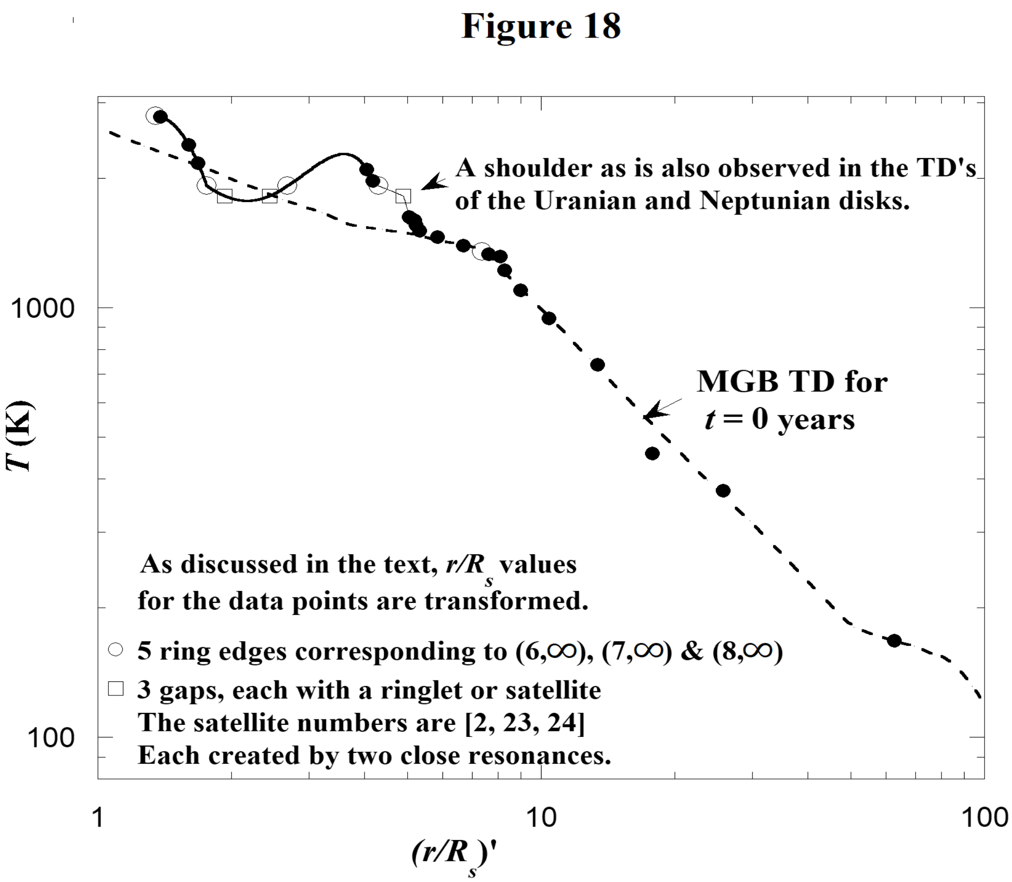

With the determined values of $C_1' = 1.080\text{K}\cdot\text{cm}$ and $C_2' = -462\ \text{cm}^{-1}$ substituted into Eq. 7 we have

$$T = 1.08\text{K}\cdot\text{cm}\ (E_p - 462\text{cm}^{-1}), \qquad (9)$$

In section 2.6 we compared the empirically determined $T(E_p)$ (Eq. (6a)) for the Uranian satellite investigation to the theoretical $T(E_p)$ (Eq. (5)). These equations are

$$T = (hc/k)(E_p - \Delta) \qquad (5)$$

and
$$T = 1.609(hc/k)(E_p - 3720\ \text{cm}^{-1}). \quad \text{Uranian satellites} \qquad (6a)$$

Similarly we now compare the empirically determined $T(E_p)$ (Eq. (9)) for the Saturnian satellite investigation to Eq. (5) by writing Eq. (9) in terms of the factor hc/k. The result is

$$T = 0.751(hc/k)(E_p - 462\text{cm}^{-1}), \qquad \text{Saturnian satellites} \qquad (9a)$$

where $0.751(hc/k) = C_1' = 1.080$ K·cm.

The leading constants (1.609 and 0.751) on the right sides of Eqs. (6a) and (9a) are both in reasonable agreement with the leading constant (1) on the right side of the theoretical relationship Eq. (5). However the fact that the two empirical constants differ by a factor of 2 is interesting. As mentioned before Appendix 3 contains the derivation of Eq. (5) for the case of A and B colliding and associating to form AB. It also includes a similar derivation for a relationship between T and E_p that involves third body assisted stimulated radiative molecular association (3rdBA SRMA). The result is

$$T = (hc/2k)(\,E_p - \Delta). \qquad (10)$$

Note the additional factor or 2 in the denominator of Eq. (10) compared to Eq. (5) above.

We comparing (Eq. (9)) to Eq. (10) by rewriting Eq. (9) in terms of the factor $hc/2k$. The result is

$$T = 1.502(hc/2k)(E_p - 462\text{cm}^{-1}), \qquad \text{Saturnian satellite} \qquad (9b)$$

where $1.502(hc/2k) = C_1' = 1.080$ K·cm.

The leading constant 1.502 in Eq. (9b) is in agreement with the leading constant of 1.609 in Eq. (6a). The agreement suggests that 3rdBA SRMA could be the key reaction that triggered satellite evolution in the Saturnian disk. The approximations made in Appendix 3 are similar for both cases presented there. Therefore if they were relaxed in both, possibly the leading constants in Eqs. (6a) and (9b) would still be in agreement.

3. FURTHER DISCUSSION AND CONCLUSIONS

If the collection of matter that leads to satellites in protoplanetary disks were mainly due to the force of gravity we would not expect the plots of Uranian satellite orbital radii vs. Jovian satellite orbital radii (Fig. 1) and Uranian satellite orbital radii vs. Neptunian satellite orbital radii (Fig. 2) to be linear. Also this investigation indicates that satellite migration is not a large factor in the evolution of planetary systems unless it is a uniform effect without satellites crossing orbits.

The empirically determined value for $\Delta = 3720$ cm^{-1} in Eq. (6a) may be helpful in the identification of the reactants A and B. The energy Δ is associated with a transition the molecule AB undergoes during the molecule's association. Black and van Dishoek (1987) list transition energies and relative spectral intensities in H_2. The (1,0)O(3) transition has an energy 3568 cm^{-1} and spectral intensity considerably higher than all other transitions near it in the spectrum. The energies (3720 and 3568 cm^{-1}) are in reasonable agreement. Similarly $\Delta = 462$ cm^{-1} in Eq. (9b) is in reasonable agreement with the transition energy 354 cm^{-1}, associated with the (0,0)S(0) transition in H_2, which has the largest spectral intensity in the H_2 spectrum (Black and van Dishoek 1987). Furthermore, Latter and Black (1990) study the formation of H_2 by radiative association. The reaction mechanism in their study is similar to SRMA except it is without stimulation. They show their mechanism requires a stabilizing photon be emitted by the H_2 during its formation. In the present model outlined in section 2.6 the stabilizing photon's energy is $E_p = |\Delta K| + \Delta$, where Δ is possibly the energy of the (1,0)O(3) or (0,0)S(0) transition in H_2.

The Colombo, Maxwell and Encke Gaps and their ringlets are produced by two closely spaced resonances associated with $E_p(5,7)$ and $E_p(6,11)$. The two together seemingly caused resonances that were strong enough to clear the gap regions and produce ringlets. Without this fortunate situation and without the well defined positions of ring edges associated the series limit $E_p(7,\infty)$, it would be impossible to determine the shape of the Saturnian Disk TD in the region of the C ring.

The present model predicts resonance rings are created early in the evolution of the Uranian and Saturnian protosatellite disks. Furthermore it seems that the matter that forms satellites is efficiently collected in these rings. If these are true, the accretion time scale is most certainly shortened from what it would be if no resonance rings existed.

The smoothness of the Uranian disk PED in Figs. 5a and 5b supports the model presented in this paper. The only point on the PED noticeably displaced corresponds to ring η. As pointed out in subsection 2.2.b this displacement could be due to gravitational resonant interaction with the satellite Cressida (Chancia et al. 2017). Also supporting the present model is the good quality of the fits of the three TD's determined in this investigation for the Uranian, Jovian and Neptunian disks to the Mousis (2004) TD (see Fig. 10) as well as the Saturnian disk TD fit to the Mousis, Gautier and Bockelee-Moran (2002) TD (see Fig. 17).

Results of the present investigation indicate rings of Saturn developed at the same time all its regular satellites developed. This is in conflict with findings from the Cassini spacecraft. Cassini measurements reveal a lower than expected total ring mass which in turn suggests the rings are only 10-100million years old (Iess et al. 2019).

Interestingly this investigation indicates the possibility that the quantum nature of matter has put its stamp not only on atomic but also and planetary systems.

ACKNOWLEDGMENTS

I would like to thank John Hogan for instilling in me an interest in stellar and planetary systems a long time ago. I also would like to thank members of the Allegheny College Physics Department for supporting my studies in this area for many years especially Professors Richard Brown and James (Jamie) Lombardi Jr. Many thanks to Jamie for his editorial assistance with this paper and for suggesting that the (hc/k) and (hc/2k) be included in Eqs. (6a) and (9b) for easier comparison of various equations. Also, many thanks to Jerry Staub for reading and commenting on various versions of this present paper and to Jim Fitch for recently reviving my desire to continue working in this area. I also acknowledge the tremendous amount of experimental and theoretical work carried out by others that is essential for this investigation.

REFERENCES

Appenzeller, I., and R. Mundt 1989. T Tauri stars. Astron. Astrophys. Rev. 1 291-334.

Augustovičová L., V. Špirko, W. P. Kraemer and P. Soldán 2013. Radiative association of He^{+}_{2} Revisited. A&A. 553

Black J., and E. F. van Dishoeck 1987. Fluorescent Excitation of Interstellar H_2. ApJ. 322 412-449.

Chancia R, O., M.W. Hedman, and R. G. French 2017, Weighing Uranus' Moon Cressida with the η Ring. AJ. 154:153 1-8.

Dalgarno A., and S. Lepp 1987. Chemistry in the early universe. I.A.U.S. 120 109-120.

Draine B. T., and F. Bertoldi 1996. Structure of stationary photodissociation fronts. ApJ. 468 269-289.

Elliot J. L. 1979. Stellar occultation studies of the solar system. Ann. Rev. Astron. and Astrophys. 17 445-475.

Farinella P., F. Marzari, and S. Matteoli 1997. The Disruption of Hyperion and the origin of Titan's atmosphere. AJ. 113 2312-2316.

Fraser H. J., M. R. S, McCoustra, and D. A. Williams 2002. The molecular universe. Astron. Geophys. 43 10-18

French R. G., P. D. Nicholson, C. C. Porco and E. A. Marouf 1991. Dynamics and structure of the uranian rings. In *Uranus* (J. T. Bergstralh, E. D. Miner and M. S. Matthews Eds.) pp. 327-409. Univ. of Arizona Press, Tucson.

French R., C. Mcghee-French, P. Nicholson, M. Hedman, N. Rappaport, E. Marouf, P. Longaretti, J. Hahn 2020. Unusual One-Armed Density Waves in the Cassini Division of Saturn's Rings. Icarus. 339, pp.113600. 10.1016/j.icarus.2019.113600. hal-02404628

Hedman M. M., J. A. Burns, M. S, Tiscareno,C. C. Porco, G. H. Jones, E. Roussos, N. Krupp, C. Paranicas and S. Kempf 2007a. The source of Saturn's G ring. Science. 317 653-656

Hedman M. M., J. A. Burns, M. R. Showalter, C. C. Porco, P. D. Nicholson, A. S. Bosh, M. S. Tiscareno, R. H. Brown, B.J. Buratti, K. H. Baines and R. Clark 2007b. Saturn's dynamic D ring. Icarus. 188 89-107

Hartmann, L., S. Kenyon, and P. Hartigan 1993. Young stars: episodic phenomena, activity and variability. In Protostars & Planets III. (E. H. Levy and J. I. Lunine, Eds.) Univ. of Arizona Press. pp. 497-518.

Herbig, G. H. 1977. Eruptive phenomena in early stellar evolution. ApJ 217 693-715.

Herczeg G. J., J. L. Linsky, F. M. Walter, G. F. Gahm, and C. M. Johns-Krull 2006. The origins of fluorescent H_2 emission from T Tauri stars. AAS. 165 256-282.

Iess L., B.Militzer, Y. Kaspi, P. Nicholson, D. Durante, P. Racioppa, A. Anabtawi, E. Galanti, W. Hubbard, M. J. Mariani, P. Tortora, S. Wahl, M. Zannoni 2019. Measurement and implications of Saturn's gravity field and ring mass. Science 364

Jerousek R. G., J. E. Colwell, M. M. Hedman, R. G. French, E.A. Marouf, L. W. Esposito, P. D. Nicholson 2020. Saturn's C ring and Cassini division: Particle sizes from Cassini UVIS, VIMS, and RSS occultations. Icarus. 344, pp.113565

JPL 1999. https://www.jpl.nasa.gov/images/epsilon-ring-of-uranus via the Internet. Accessed January 2022

Kwan J., and W. Fischer 2011. Origins of the H, He I and Ca II line emission in classical T Tauri stars. MNRAS. 411 2383-2425.

Lin D. N. C., and J. Papaloizou 1985. On the dynamical origin of the solar system. In Protostars & Planets II (D. C. Black, and M. S. Matthews Eds.) pp. 981-1072. Univ. of Arizona Press, Tucson. Referred to as L&P(1985) in the present paper.

Lombardi J. C. 2015a. Stimulated Radiative Molecular Association in the Early Solar System: Orbital Radii of Satellites of Uranus, Jupiter, Neptune, and Saturn. https://arxiv.org/abs/1506.00268 via the Internet. Accessed

Lombardi J. C. 2015b. Stimulated Radiative Molecular Association in the Early Solar System II**.** Orbital Radii of the Planets and Other Satellites of the Sun https://arxiv.org/abs/1508.06598 via the Internet. Accessed January 2022

Martini P., K. Sellgren and D. L. DePoy 1999. Near-infrared spectroscopy of molecular hydrogen emission in four reflection nebulae: NGC 1333, NGC 2023, NGC 2068, and NGC 7023. ApJ. 526 772-787.

Mousis, O., D. Gautier and D. Bockelée-Moran 2002. An evolutionary turbulent model of Saturn's subnebula: Implications for the origin of the atmosphere of Titan. Icarus 156 162-175.

Mousis, O. 2004. Modeling the thermodynamical conditions in the uranian subnebula – Implications for regular satellite compositions. A&A 413 373-380.

Mousis, O., and Y. Alibert 2006. Modeling the jovian subnebula. II. Composition of regular satellite ices. A&A 448 771-778

NASA 2021, Lunar and Planetary Science. Available at: https://nssdc.gsfc.nasa.gov/planetary/ via the Internet. Accessed throughout 2021.

NASA 2022, Planetary Data System. Available at: https://pds-rings.seti.org/saturn/saturn_tables.html via the Internet. Accessed January 2022

Planetary Society 2021, Available at: https://planetary.org/space-images/panoramic-scan-across via the Internet. Accessed November 2021.

Stancil P. C. and A. Dalgarno 1997. Stimulated radiative association of Li and H in the early universe. ApJ. 479 543-546.

Turk M. J., P. Clark, S. C. O. Glover, T. H. Greif, T Abel, R. Klessen, and V. Bromm 2011. Effects of varying the three-body molecular hydrogen formation rate in primordial star formation. ApJ. 726:55 (11pp)

APPENDIX 1
Mousis Temperature Distributions

Section A1.a. Reproduction of Mousis TD's in Figure 6

Figure 6 includes reproductions of three TD's from Mousis (2003). These are the three TD's that are labeled $t = 1\text{x}10^4$, $2\text{x}10^4$ and $5\text{x}10^4$ years. The graphic editor GIMP is used to determine the coordinates of critical points in Figure 1 of Mousis (2003). Each of these TD's is represented mostly by straight line segments when plotted using logarithmic scales. The only exception is the curved, very top portion of the $t = 1\text{x}10^4$ TD which is not reproduced in Figure 6 of the present investigation. Each of the straight line segments in Figure 6 is of the form $T = \beta r^{\,n}$, where r is the radial coordinate in the disk and β and n are constants that determine the position and slope of the straight line segments. The various values of β and n are used to reproduce the Mousis TD's in Figure 6.

Section A1.b. Construction of Dashed TD's in Figure 6

Similarities among the three Mousis TD's make it possible to construct the two dashed TD's in Fig.6.

1. The top segment of each Mousis TD connects to the top of its middle segment at ***approximately*** the same temperature. And the bottom segment of each TD connects to the bottom of its middle segment at ***approximately*** the same temperature. Call these temperatures T_1 and T_1' in the TD for which $t = 1\text{x}10^4$ years.
2. Each segment in a TD is nearly parallel to a corresponding segment in the other two TD's. I.e. they have nearly the same n. Call these n values, n_1, n_2 and n_3 in the TD for which $t = 1\text{x}10^4$ years.

Because the dashed TD's in Figure 5 are close to the Mousis $t = 1\text{x}10^4$ year TD, the approximate similarities mentioned in point 1 above can be taken to be nearly exact. Now each dashed TD is determined as follows.

1. Temperatures where its segments connect are T_1 and T_1', just as in the Mousis TD for which $t = 1\text{x}10^4$ years.
2. Its three segments have n values, n_1, n_2 and n_3 just as in the Mousis TD for which $t = 1\text{x}10^4$ years.
3. The value of β for the middle segment of the dashed TD is taken to be a few percent larger than what it is in the Mousis TD for which $t = 1\text{x}10^4$ years. Appendix 2 explains how t is determined from this new β.

4. The two radial coordinates r_1 and r_1', for the points where segments connect, can be found by applying the relationship $T = \beta r^n$ to each end of the middle segment where T is either T_1 or T_1'.
5. Repeated use of the equation $T = \beta r^n$, determines the β values for the rest of the segments.
6. Knowing β and n for each segment determines the dashed TD.

APPENDIX 2

Finding the Time When the Uranian Satellites Begin Their Evolution

Figure A2
The graph of log(*t*) vs log(β_m) is linear.

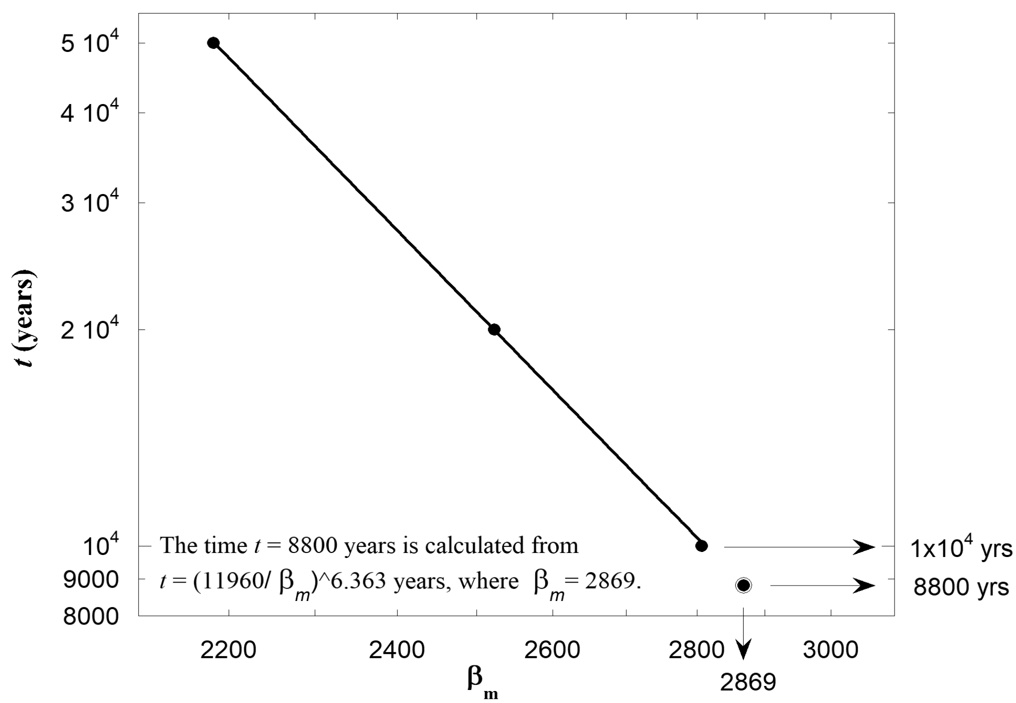

The three TD's in Figure 6 associated with $t = 1 \times 10^4$, 2×10^4, and 5×10^4 years are all reconstructed from Figure 1 in Mousis (2003). Each segment of these TD's is characterized by an equation of the form $T = \beta r^n$, as discussed in Appendix 1. Figure A2 utilizes the values of β for the three middle segments for the reconstructed Mousis TD's: we are calling them β_m. The values of β_m are measured, as described in Appendix 1, to be 2807, 2523 and 2183 for times $t = 1 \times 10^4$, 2×10^4, and 5×10^4 years respectively. Because the graph of log(t) vs log(β_m) is linear, the relationship between t and β_m has the form

$$t = \text{constant x } \beta_m^{-P}$$

and the best fit to the data is $t = (11960/\beta_m)^{6.363}$. Uranian satellites begin their evolution at a time when the TD for the Uranian protosatellite disk is characterized $\beta_m = 2869$. We extrapolate the graph in Figure A2 to earlier time by substituting this value of β_m into the above equation. The result for t is $t_0 = 8800$ years, the time when the Uranian satellites begin their evolution. For the other dashed TD, β_m is arbitrarily taken to be 6% larger than the β_m in the Mousis TD for which t =1 x 10^4 years. The t value for the other dashed TD is found in the same way to be 6900 years.

APPENDIX 3

The Relationship Between T and E_p

Section A3.a. Case 1: Protosatellite Disks of Uranus, Jupiter and Neptune

We use the model presented in section 2.6 to derive T as a function of E_p. The following relationship, Eq. (4) in the main text, is an expression of the SRMA that is key to the present discussion,

$$A + B + hv \rightarrow AB + 2hv. \qquad (4)$$

In this reaction A and B, with momenta $\boldsymbol{p_A}$ and $\boldsymbol{p_B}$, collide to form AB with the momentum $\boldsymbol{p_{AB}}$. A more accurate calculation to determine $T(E_p)$ would include the realistic effect of a range of possible angles between $\boldsymbol{p_A}$ and $\boldsymbol{p_B}$. before the collision. However a likely angle between $\boldsymbol{p_A}$ and $\boldsymbol{p_B}$ is 90º. For the sake of simplifying the calculation, we calculate $T(E_p)$ for the single case of $\boldsymbol{p_A}$ and $\boldsymbol{p_B}$ being perpendicular

$$p_{AB}^2 = p_A^2 + p_B^2. \qquad (A3.1)$$

Also the momentum of p_{AB} is about 30,000 times greater than momentum of the photon created during the collision. Therefore there is no need to account for the photon's momentum in Eq. (A3.1). The kinetic energies of A, B and AB are $K_A = ½p_A^2/m_A$, $K_B = ½p_B^2/m_B$, and $K_{AB} = ½p_{AB}^2/m_{AB}$, where m_A, m_B, and m_{AB} are the respective masses and m_{AB} has a value that is extremely close to $m_A + m_B$. With these expressions, Eq. (A3.1) becomes

$$m_{AB} K_{AB} = m_A K_A + m_B K_B \qquad (A3.2)$$

There is likely a range of kinetic energies associated with the A's and B's that participate in SRMA resonance. However we simplify our calculation by defining K_{mp} as the most probable kinetic energy of the A's and B's that participate. The most probable speed in a Maxwell-Boltzmann distribution is $v_{\mathrm{mp}} = (2kT/m)^{½}$, where m is the particle mass. Particles with this speed have a kinetic energy of kT and we take $K_A = K_B = K_{\mathrm{mp}} = kT$.

All of this together yields $\quad K_{AB} = K_{\mathrm{mp}} (m_A + m_B)/m_{AB} = K_{\mathrm{mp}},$ (final kinetic energy) (A3.3)

where $(m_A + m_B)/m_{AB}$ is extremely close to unity.

Also $\quad K_A + K_B = 2K_{\mathrm{mp}}$ (initial kinetic energy) (A3.4)

and the change in kinetic energy of the system during the association that creates AB is

$$\Delta K = (K_{AB} - (K_A + K_B)) = - K_{\mathrm{mp}} = - kT\,. \qquad (A3.5)$$

By conservation of energy, the energy of the created photon (hv) is

$$E_p = |\Delta K| + \Delta, \qquad (A3.6)$$

where the energy Δ, accounts for a transition that may occur in the molecule during its association.

From Eqs. (A3.5) and (A3.6)

$$T = (1/k)(E_p - \Delta). \quad \text{(A3.7)}$$

In the analysis E_p's are in the units of wave numbers. To account for this we multiply the right side of Eq. (A3.7) by hc where h is Planck's constant and c is the speed of light. Also the value of (hc/k) is 0.014388 K·m = 1.4388 K·cm. Therefore we have

$$T = (hc/k)(E_p - \Delta) . \quad \text{(A3.8)}$$

This is also Eq. (5) in the main text.

A3.b. Case 2: Third Body Assisted Stimulated Radiative Molecular Association as the Possible Key Reaction that Triggered Satellite Evolution in the Saturnian disk

For Saturn's disk, Eq (9) in section 2.8 is determined by adjusting the parameters a, C_1' and C_2' so that T's calculated from Eq. (7) fit the MGB (2002) TD for which t = 0 years. The result is

$$T = (1.080 \text{ K·cm})(E_p - 462 \text{ cm}^{-1}) \qquad \text{(from fit).} \qquad (9)$$

Because the constant 1.080 K·cm in Eq. (A3.8) is about one half the constant 2.315 K·cm in Eq. (6) for Uranus's disk, we expect the key SRMA reaction for Saturn's disk to involve a different number of atoms or molecules. Third body assisted association (Fraser, McCoustra, and Williams 2002 & Turk et. al. 2011) is characterized by

$$A + B + C = AB + C. \quad \text{(A3.9)}$$

In this reaction C assists in the association of A and B to form AB. We propose the following reaction which is a combination of Eqs. (4) and (A3.9).

$$A + B + C + h\nu \rightarrow AB + C + 2h\nu. \quad \text{(A3.10)}$$

In Eq. (A3.10) both C and $h\nu$ assist the radiative molecular association. Therefore Eq. (A3.9) characterizes third body assisted stimulated radiative molecular association. This is actually a 4-body interaction because of the requirement that a photon also must participate in the collision. Generally speaking 4-body interaction are less likely than 3-body interactions. However in this case the photon on the left side of Eq. (A3.10) is a readily available resonant photon with exactly the correct direction of motion to participate in a collision which in turn further enhances resonance. This should make the 4-body interaction more likely than it would otherwise be.

We now derive a formula that is close to the empirical Eq. (9) found for Saturn's disk. We make the simplifying approximation that C moves off in the same direction and at the same speed as does AB after the collision. But also physically speaking, it seems likely for C to travel with AB in order for C to assist in the association of A and B to make AB. So the magnitude of the final momentum of the system is equal to the sum of the magnitudes of the momenta of AB and C. In addition to formulas we used in Case 1 above, we have $K_{ABC} = \frac{1}{2}p_{ABC}^2/m_{ABC}$, where K_{ABC} is the sum of the kinetic energies of AB and C, (i.e. the final kinetic energy of the system) and p_{ABC} is the magnitude of the system's momentum. Also, $m_{ABC} = m_{AB} + m_C$, where m_C is the mass of C and K_C is its kinetic energy before the collision.

The vectors $\boldsymbol{p_A}$, $\boldsymbol{p_B}$ and $\boldsymbol{p_C}$ are the momenta of A, B and C before they collide. Again, while realizing there is likely a range of angles between these vectors, we simplify the calculation by taking these vectors to be perpendicular for resonant reactions. We therefore consider A, B and C approaching each other as if each one is moving along one of the axes in a three-dimensional Cartesian coordinate system. Therefore

$$(p_{ABC})^2 = p_A^2 + p_B^2 + p_C^2, \tag{A3.11}$$

and

$$(m_{AB} + m_C)\,K_{ABC} = m_A K_A + m_B K_B + m_C K_C \tag{A3.12}$$

Assuming again that $K_A = K_B = K_C = K_{\mathrm{mp}}$ and $(m_A + m_B + m_C)/(m_{AB} + m_C) = 1$ we have

$$K_{ABC} = K_{\mathrm{mp}}\,(m_A + m_B + m_C)/(m_{AB} + m_C) = K_{\mathrm{mp}} \text{ (final kinetic energy)} \tag{A3.13}$$

Also

$$K_A + K_B + K_C = 3K_{\mathrm{mp}} \quad \text{(initial kinetic energy)} \tag{A3.14}$$

And

$$\Delta K = (K_{ABC} - (K_A + K_B + K_C)) = -2K_{\mathrm{mp}} = -2kT \text{ (where } K_{\mathrm{mp}} = kT). \tag{A3.15}$$

As in the last derivation

$$E_p = |\Delta K| + \Delta \tag{A3.16}$$

And this time

$$T = (hc/2k)(E_p - \Delta) \tag{A3.17}$$

Note the 2 in the denominator of the first factor on the right side of Eq. (A3.10). A 2 does not appear in Eq. (A3.8)

Appendix 4

The Construction of the Approximate Curve Used for the B Ring Portion of the PED in Figs. 13 and 14

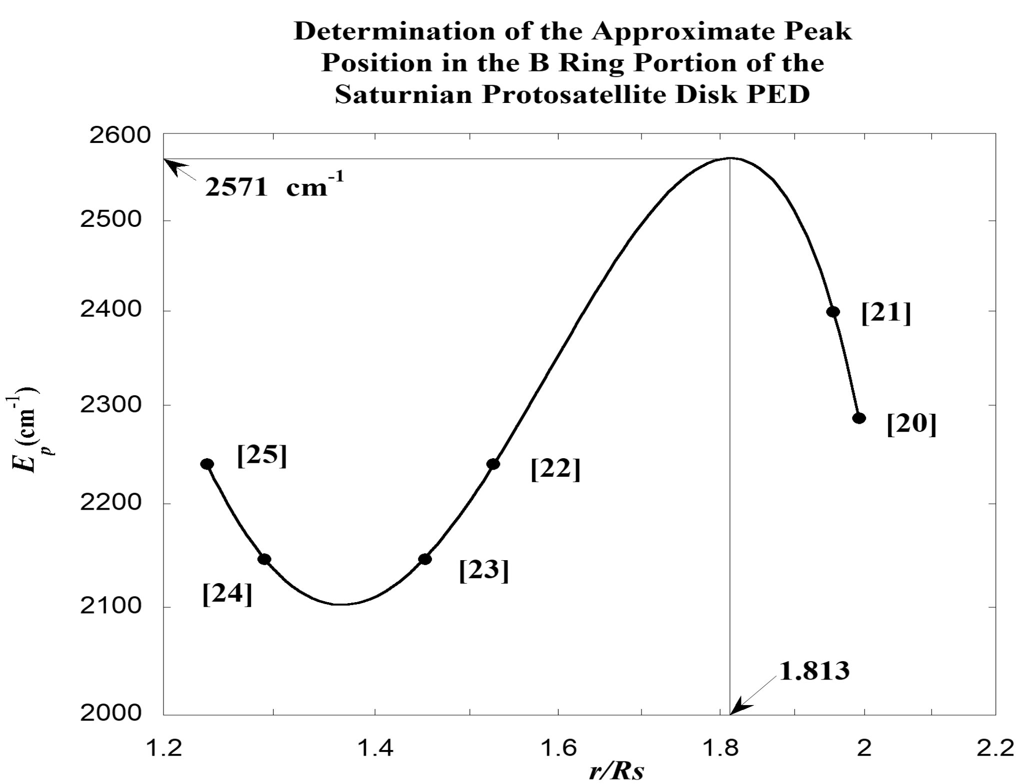

The present investigation does not indicate that any well defined resonance rings contribute to the creation of the B ring portion of the PED associated with Saturn's protoplanetary disk. Section 2.7.c indicates the B ring evolved from of a number of wide resonance rings. Therefore it is necessary to make a reasonable approximation for the shape and magnitude of the PED in this region. This is achieved by (1) assuming the PED's value and slope are continuous across the boundary between the C and B rings and (2) assuming the PED passes through the two key points associated with the Huygens and Laplace ringlets. The four points that are associated with the C ring and the two points associated with the Huygens and Laplace ringlets are all fitted with one continuous function in the form of a cubic polynomial. This curve is used for the curve of the PED in the figure above and to fit the C ring and the Cassini Division as well as approximate the B ring in Figs. 13 and 14 in the main text.

An equation for the cubic polynomial in the figure is

$$E_p = 2571 - 7060(r/R_s - 1.8130)^2 - 10540(r/R_s - 1.8130)^3.$$

The curve has a maximum value of E_p = 2571 cm^{-1} at r/R_s = 1.8130 and a minimum value of E_p = 2102 cm^{-1} at r/R_s = 1.3666.

Italicized r/R_s and E_p data are used to make the fitted points in the graph.

Satellite or Ring Edge Name	[*i*][a]	r/R_s [b]	n_f, n_i [c]	$E_p(n_f, n_i)$ [c] (cm^{-1})
Inner Edge C ring	***[25]***	***1.239***	*7,∞*	***2239.5***
Titan ringlet in Colombo Gap	[24]		5,7	2149.9
Titan ringlet in Colombo Gap	[24]		6,11	2141.3
Average Titan ringlet E_p's	***[24]***	***1.292***		***2145.7***
Maxwell ringlet in Maxwell Gap	[23]		6,11	2141.3
Maxwell ringlet in Maxwell Gap	[23]		5,7	2149.9
Average Maxwell ringlet E_p's	***[23]***	***1.452***		***2145.7***
Outer Edge C ring	***[22]***	***1.526***	*7,∞*	***2239.5***
Inner Edge B ring		1.526		
Outer Edge B ring		1.950		
Huygens ringlet in Huygens Gap	***[21]***	***1.955***[d]	***6,13***	***2398.9***
Laplace ringlet in Laplace Gap	***[20]***	***1.992***[d]	***6,12***	***2286.2***

[a] Indices in Tables 8 and 9 and Fig. 14

[b] Orbital radii of satellites and rings in units of the equatorial radius of Saturn and are from NASA (2021) except as otherwise noted.

[c] The quantum numbers that define transitions in the hydrogen atom and photon energies associated with these transitions.

[d] French et al. (2020) Fig. 2 and NASA (2022)